# Vortex state in *d*-wave superconductors with strong paramagnetism: Transport and specific heat anisotropy

A. B. Vorontsov
*Department of Physics, Montana State University, Bozeman, Montana 59717, USA*

I. Vekhter
*Department of Physics and Astronomy, Louisiana State University, Baton Rouge, Louisiana 70803, USA*

(Received 19 January 2010; revised manuscript received 10 March 2010; published 31 March 2010)

We analyze the combined effect of orbital and Pauli depairing on the superconducting state, and apply the results to the heavy fermion $CeCoIn_5$. We find that (a) standard extrapolation based on the slope of $H_{c2}(T)$ in the vicinity of the transition temperature does not always give accurate values of the orbital upper critical field; (b) critical value of the Maki parameter, $\alpha$, which determines onset of the first order transition, depends on the Fermi surface shape and the symmetry of the gap and is $\alpha^* \approx 3$ for $CeCoIn_5$; and (c) the anisotropy of the thermodynamic and transport coefficients in the low-temperature, low-field part of the phase diagram is essentially insensitive to the Zeeman field and can be used to determine the nodal directions in Pauli-limited superconductors. The latter result confirms the finding of the $d_{x^2-y^2}$ order parameter $CeCoIn_5$.

DOI: 10.1103/PhysRevB.81.094527 PACS number(s): 74.25.fc, 74.20.Rp, 74.25.Bt

## I. INTRODUCTION

Magnetic field is one of the most widely utilized and powerful probes of the unconventional superconducting state. It couples to momentum and spin of the quasiparticles, via the orbital and Zeeman mechanisms, respectively, and therefore can be used to probe both the momentum dependence of the order parameter and the spin structure of the Cooper pairs.

In singlet superconductors both mechanisms are detrimental to superconductivity. The orbital coupling of the Cooper pair motion to the vector potential of the field leads, in type-II superconductors, to the appearance of a mixed state with partial field penetration. The Cooper pair supercurrents and the order parameter are spatially modulated and form an array of Abrikosov vortices. The upper critical field at which the second order transition into the normal state occurs is given $H_{c2}^{orb} \sim \Phi_0/2\pi\xi^2$, where $\Phi_0$ is the flux quantum and $\xi$ is the superconducting coherence length.[1] For unconventional superconductors, below that field the number of the quasiparticles outside of the superconducting condensate and, consequently, entropy-sensitive properties, such as the specific heat or thermal conductivity, depend on the relative orientation of the field with respect to zeroes (nodes) or deep minima in the energy gap.[2–12] The corresponding measurements have been extensively used to determine the symmetry of the superconducting state[13–25] with the heavy fermion $CeCoIn_5$ and $CeIrIn_5$ being two examples where a reasonably detailed comparison of theory and experiment was carried out.[9–11,15,21] Crucially, the anisotropic signal changes sign depending on the values of $T$ and $H$ in the superconducting phase diagram so that either minima or maxima correspond to the direction of the field along the nodes.[9–11] Consequently, a detailed theoretical analysis is required for the interpretation of the experimental data. So far, such an analysis has only been carried out for purely orbital coupling.

At the same time measurements on $CeCoIn_5$ clearly show that the second suppression mechanism, depairing due to Pauli spin polarization, is important in this compound.[26–28] From the theory perspective, magnetic field aligns the spins of the unpaired electrons while the singlet Cooper pairs cannot take advantage of the lower energy offered by a spin-polarized state. As a result, in the absence of the orbital effects, the normal state is energetically favorable above the Pauli critical field $H_P(T=0)=\Delta_s/\sqrt{2}\mu_B$ (for isotropic superconductors, see below), where $\Delta_s$ is the superconducting gap and $\mu_B=\hbar e/2m_e c$ is the Bohr magneton.[29,30] The normal state is reached via a second order transition at $T>T_P^* \sim 0.56T_c$ and a first order transition at low temperatures $0<T<T_P^*$. In the absence of strong anisotropy of the spin-orbit coupling, the number of unpaired electrons at $H<H_P$ does not depend on the field orientation and therefore whenever this mechanism is dominant it is not immediately obvious how efficient the field is for determination of the gap symmetry and when exactly the inversion of the anisotropy pattern takes place.

Under most circumstances the orbital suppression mechanism dominates, $H_{c2}^{orb} \ll H_P$. Pauli limiting is important in thin films and other quasi-two-dimensional materials, when the orbital coupling is inefficient.[31–33] In strongly layered materials even at relatively low fields the Zeeman pairbreaking effect may complicate the extraction of the nodal contribution to the specific heat.[3,34] Even in relatively three-dimensional systems, if the characteristic electron velocity (Fermi velocity) is low and hence the coherence length is short, as it is in many heavy fermion and other correlated superconductors, the orbital upper critical field is high, and can be comparable to the Pauli limiting field. The question of what the vortex state anisotropies can tell us about the superconducting gap symmetry in this situation has not been explored before and is the subject of this paper.

We consider a model relevant to $CeCoIn_5$.[26,27,35] The situation when the orbital and Pauli pairbreaking mechanisms are comparable was considered early on by Gruenberg and Gunther[36] and by Maki[37] for an *s*-wave superconductor with spherical Fermi surface (FS). $CeCoIn_5$ has *d*-wave gap symmetry with the main *f*-electron containing Fermi surface

 

sheet open along the $c$ axis.[38–41] Consequently, as our first task, we compute the upper critical field as a function of temperature for different orientations. We extend previous calculations[42–44] to the Fermi surface in the shape of a corrugated cylinder that gives the correct normal state resistivity anisotropy and find the temperature $T^*$, below which the normal to superconducting transition becomes first order. One of our main findings is that the commonly used criterion for determining the dominant Pauli limiting regime via the Maki parameter,[37] $\alpha=\sqrt{2}H_{c2}^{orb}/H_P>1$ is quantitatively incorrect and depends on the symmetry of the gap and on the shape of the Fermi surface.

Second, we analyze the anisotropy of the specific heat and the thermal conductivity under rotated magnetic field across the $T$-$H$ phase diagram including the effects of Pauli limiting. Since the precise details of the behavior of the anisotropy are used to infer the gap symmetry from experiment, this extension is critical for justifying $d_{x^2-y^2}$ symmetry in $CeCoIn_5$. We show that even moderately high Pauli effect has little influence on the low-temperature and low-field part of the phase diagram whereas its consequences near the upper critical field are considerable.

## II. QUASICLASSICAL FORMULATION

### A. Basic equations for superconductors under Zeeman and orbital field

We use the quasiclassical formalism[45,46] at real frequencies, $\varepsilon$, which allows to carry out calculations for arbitrary temperature and field and to self-consistently include effects of the field and impurities on the order parameter. The quasiclassical transport equation for the matrix Green's function in particle hole and spin space, $\hat{g}$, has the form[47]

$$\left[\left(\varepsilon+\frac{e}{c}\mathbf{v}_f(\hat{\mathbf{p}})\mathbf{A}(\mathbf{R})\right)\hat{\tau}_3-\mu\mathbf{B}\cdot\hat{\mathbf{S}}-\hat{\Delta}(\mathbf{R},\hat{\mathbf{p}})-\hat{\sigma}_{imp}(\mathbf{R};\varepsilon),\quad \hat{g}(\mathbf{R},\hat{\mathbf{p}};\varepsilon)\right]+i\mathbf{v}_f(\hat{\mathbf{p}})\cdot\nabla_{\mathbf{R}}\hat{g}(\mathbf{R},\hat{\mathbf{p}};\varepsilon)=0. \tag{1}$$

Here $[E_1,E_2]$ denotes a commutator, and we carried out the standard[48] separation of the center-of-mass coordinate, $\mathbf{R}$, and the momentum of the relative motion, $\mathbf{p}$, so that the Fermi velocity depends on the position on the Fermi surface, $\mathbf{v}_f(\hat{\mathbf{p}})$. The orbital coupling is via the electron charge and the vector potential, $\mathbf{A}(\mathbf{R})$, and the Zeeman term, $\mu\mathbf{B}\cdot\hat{\mathbf{S}}$, is proportional to the electron's magnetic moment $\mu=(\mathfrak{g}/2)\mu_B$ with $\mathfrak{g}$ factor as a material-specific parameter and the spin matrix,

$$\hat{\mathbf{S}}=\begin{pmatrix}\boldsymbol{\sigma} & 0\\ 0 & \boldsymbol{\sigma}^*\end{pmatrix} \tag{2}$$

with $\boldsymbol{\sigma}$ the usual vector of Pauli matrices. The (retarded) Green's function in particle hole and spin space,

$$\hat{g}^R=\begin{pmatrix}g+\mathbf{g}\boldsymbol{\sigma} & (f+\mathbf{f}\boldsymbol{\sigma})i\sigma_y\\ i\sigma_y(f'+\mathbf{f}'\boldsymbol{\sigma}) & -g+\mathbf{g}\boldsymbol{\sigma}^*\end{pmatrix}, \tag{3}$$

satisfies normalization $\hat{g}^2=-\pi^2\hat{1}$. Equation (1) is complemented by two other equations. One is the used to determine the impurity self-energy, which we treat in the self-consistent $t$-matrix approximation,[49] $\hat{\sigma}_{imp}(\mathbf{R};\varepsilon)=n_{imp}\hat{t}(\mathbf{R};\varepsilon)$, with

$$\hat{t}(\mathbf{R};\varepsilon)=u\hat{1}+uN_0\langle\hat{g}(\mathbf{R},\hat{\mathbf{p}};\varepsilon)\rangle_{\hat{\mathbf{p}}}\,\hat{t}, \tag{4}$$

where $N_0$ is the density of states (DOS) at the Fermi level, and angle brackets denote Fermi surface average. In writing this equation we assumed nonmagnetic isotropic scattering with the individual impurity potential strength $u$ so that the impurity self-energy does not have any momentum dependence.[49] The second equation is the self-consistency condition on the order parameter which relates it to the off-diagonal, in particle-hole space, component of the Green's function. Before we write it explicitly, however, it is convenient to rewrite the function $\hat{g}$ in a different representation.

Recall that we are interested in the regime $H\gg H_{c1}$, when the vortices form an Abrikosov lattice and are considering strongly type-II superconductors. In this case the internal field $\mathbf{B}$ is essentially uniform and equal to the applied field, $\mathbf{H}$. The important point is that for a field which orientation is the same at all spatial points we can choose the spin quantization axis along the field $\mathbf{H}=H\hat{\mathbf{z}}$ and introduce for all vector quantities the notation $\mathbf{x}\cdot\boldsymbol{\sigma}=\bar{x}\sigma_z$. This choice is rigorously justified in the absence of spin-orbit interaction. In general, in heavy fermion systems the superconducting states are classified by parity, rather than true spin quantum number, and the selection of the pseudospin quantization axis along the field is justified only for high symmetry directions. We employ this simplified description hereafter with the adjustable effective $\mathfrak{g}$ factor to obtain the salient features of the behavior. Then the $4\times4$ Green's function, Eq. (1) consists of two blocks,

$$\hat{g}^R=\begin{pmatrix}g+\bar{g} & 0 & 0 & f+\bar{f}\\ 0 & g-\bar{g} & -f+\bar{f} & 0\\ 0 & f'-\bar{f}' & -g+\bar{g} & 0\\ -f'-\bar{f}' & 0 & 0 & -g-\bar{g}\end{pmatrix}, \tag{5}$$

corresponding to the spin-up and spin-down components. The impurity self-energy $\hat{\sigma}_{imp}$ assumes the same block form. Note that here our assumption of the isotropic purely potential impurities is crucial: inclusion of strongly momentum-dependent impurity scattering as well as the spin-orbit component of the scattering potential makes the problem significantly more complex, as discussed in detail in Ref. 50.

The block structure allows us to rewrite the equations for the components of the Green's function in a simple form. We explicitly introduce the equations for the two spin components, $s=\{\uparrow(+1),\downarrow(-1)\}$ via $g_s=g+s\bar{g}$ and $f_s=f+s\bar{f}$. These functions now satisfy independent quasiclassical equations

and normalization conditions, $g_s^2 - f_s f_s' = -\pi^2$, with the Zeeman energy shift $\varepsilon \to \varepsilon \mp \mu B$ for up and down spin, respectively, see also Ref. 51. Now, for example, equation for the off-diagonal part of the Green's function takes the form

$$\left\{ -2i(\tilde{\varepsilon}_s - s\mu B) + \mathbf{v}_f(\hat{\mathbf{p}}) \left[ \nabla_{\mathbf{R}} - i\frac{2e}{\hbar c}\mathbf{A}(\mathbf{R}) \right] \right\} f_s(\mathbf{R},\hat{\mathbf{p}};\varepsilon) = 2\tilde{\Delta}_s(\mathbf{R};\varepsilon) i g_s(\mathbf{R},\hat{\mathbf{p}};\varepsilon). \quad (6)$$

Here we introduced the shorthand notations $\tilde{\varepsilon}_s = \varepsilon - \Sigma_s$ and $\tilde{\Delta}_s = \Delta + \Delta_{imp,s}$ explicitly including the diagonal ($\Sigma_s$) and off-diagonal, $\Delta_{imp,s}$ components of

$$\hat{\sigma}_{imp,s}(\mathbf{R};\varepsilon) \equiv n_{imp}\hat{t}_s(\mathbf{R};\varepsilon) = \begin{pmatrix} \Sigma_s & \Delta_{imp,s} \\ -\Delta_{imp,s}^* & -\Sigma_s \end{pmatrix}. \quad (7)$$

Inversion of Eq. (4) to obtain closed-form expressions for $\Sigma_s$ and $\Delta_{imp,s}$ in terms of Green's function, scattering rate $\Gamma = n_{imp}/\pi N_0$ and phase shift $\delta_0 = \tan^{-1}(\pi u N_0)$ is done in Ref. 10. The spins mix only through the self-consistency equation for the singlet order parameter,

$$\Delta(\mathbf{R},\mathbf{k};\varepsilon) = \int_{-\Omega_c}^{+\Omega_c} \frac{d\varepsilon}{4\pi i} \tanh\frac{\varepsilon}{2T} \times \langle V(\mathbf{k},\mathbf{p})[f_\uparrow(\mathbf{R},\hat{\mathbf{p}};\varepsilon) + f_\downarrow(\mathbf{R},\hat{\mathbf{p}};\varepsilon)\rangle_{\hat{\mathbf{p}}}, \quad (8)$$

where $V(\mathbf{k},\mathbf{p})$ is the pairing potential, and $\Omega_c$ is a high energy cut-off. Equation (6) has the same form as the quasiclassical equation in the absence of Zeeman term and therefore we can utilize the existing techniques to solve for each of the two spin components independently, enforcing the self-consistency for the order parameter at the final step.

### B. Model and method of solution

We follow the approach we developed earlier[9–11,52] and solve the equations using a modified Brandt-Pesch-Tewordt (BPT) approximation.[53,54] We assume the existence of the Abrikosov vortex lattice and model the spatial dependence of the order parameter by $\Delta(\mathbf{R},\mathbf{p}) = \Delta(\hat{\mathbf{p}})\langle \mathbf{R}|0\rangle = \Delta\mathcal{Y}(\hat{\mathbf{p}})\langle \mathbf{R}|0\rangle$, where $\mathcal{Y}(\hat{\mathbf{p}})$ is the normalized ($\langle \mathcal{Y}(\hat{\mathbf{p}})^2\rangle_{\hat{\mathbf{p}}} = 1$) basis function for the irreducible representation corresponding to the chosen gap symmetry, and normalized by a proper choice of $C_{k_y}$ coefficients the spatial vortex lattice profile,

$$\langle \mathbf{R}|0\rangle = \sum_{k_y} C_{k_y} \frac{e^{ik_y\sqrt{S_f}y}}{\sqrt[4]{S_f\Lambda^2}} \tilde{\Phi}_0(x,k_y). \quad (9)$$

The magnetic length $\Lambda^2 = hc/2eB$ and

$$\tilde{\Phi}_0(x,k_y) = \Phi_0\left( \frac{x - \Lambda^2\sqrt{S_f}k_y}{\Lambda\sqrt{S_f}} \right) \quad (10)$$

is the ground-state oscillator function, and $x$ and $y$ are in the direction normal to the field.[10] Here we approximated the vortex lattice by only the superposition of the lowest oscillator wave functions, $|0\rangle$. The admixture of the higher oscillator states is small[55,56] and does not substantially affect the conclusions regarding the properties in the vortex state.[9–11,56] Hence we consider only the lowest Landau level, as reflected in Eq. (9), but with properly rescaled Fermi velocity component perpendicular to the field. For a Fermi surface rotationally invariant around the $c$ axis that we consider below[10]

$$S_f = \left[ \cos^2\theta_H + \frac{v_{0\|}^2}{v_{0\perp}^2}\sin^2\theta_H \right]^{1/2}, \quad (11)$$

$\theta_H$ is the angle between the field direction and the $c$ axis. We defined $v_{0\|}^2 = 2\langle \mathcal{Y}^2(\hat{\mathbf{p}}) v_\|^2(p_z)\rangle_{\hat{\mathbf{p}}}$, and $v_{0\perp}^2 = 2\langle \mathcal{Y}^2(\hat{\mathbf{p}}) v_{\perp i}^2(p_z)\rangle_{\hat{\mathbf{p}}}$, where $v_\|$ is the $c$-axis component of the Fermi velocity while $v_{\perp i}$ with $i = a,b$ is the Fermi velocity component in the $a$-$b$ plane. For the field in the basal plane $\theta_H = \pi/2$ and therefore $S_f = v_{0\|}/v_{0\perp}$.

The BPT approximation consists of replacing the diagonal part of the Green's function with its spatial average. It is essentially exact at $H/H_{c2} \geq 0.5$ for strongly type-II superconductors[53,57] and gives the BCS Green's function in the limit $H \to 0$, thereby providing a very good interpolation between the low- and moderate-to-high field regimes. In systems with nodes in the gap, where the states outside the vortex core give the major contribution to the thermal and transport properties, one may expect the method to continue to work even in the regime where, in a fully gapped system, the vortex core states ignored here would dominate the DOS. Indeed, in nodal superconductors the low-field range the density of states obtained via this approximation is very close to that found using the Doppler shift approach.[58] The inversion of the anisotropy in the zero-energy density of states occurs at exactly the same ratio of $H/H_{c2}$ in the BPT approach and in the solution of the microscopic Bogoliubov-de Gennes equations.[10,59] Consequently, the BPT method is well justified over a wide range of fields for unconventional superconductors.

The equations for the off-diagonal components of the Green's function are solved by introducing the ladder operators[60] as in Refs. 10 and 11, and, in conjunction with the normalization condition, for the lowest Landau level give

$$f_s = \pi \frac{1}{\sqrt{1+P}} \frac{2\sqrt{\pi}\Lambda}{|\tilde{v}_f^\perp|} W\left[ \frac{2(\tilde{\varepsilon} - s\mu B)\Lambda}{|\tilde{v}_f^\perp|} \right] \tilde{\Delta}_s,$$

$$g_s = \pi \frac{-i}{\sqrt{1+P}},$$

$$P = -i\sqrt{\pi}\left( \frac{2\Lambda}{|\tilde{v}_f^\perp|} \right)^2 W'\left[ \frac{2(\tilde{\varepsilon} - s\mu B)\Lambda}{|\tilde{v}_f^\perp|} \right] \tilde{\Delta}_s\tilde{\Delta}_s \quad (12)$$

with $\tilde{\Delta}_s(\hat{\mathbf{p}},\varepsilon) = \Delta(\hat{\mathbf{p}}) + \Delta_{imp,s}(\varepsilon)$, $W(z) = \exp(-z^2)\mathrm{erfc}(-iz)$, and

$$|\tilde{v}_f^\perp| = \left[ \frac{v_{f,x}(\hat{\mathbf{p}})^2}{S_f} + v_{f,y}^2(\hat{\mathbf{p}}) S_f \right]^{1/2}. \quad (13)$$

This closed-form solution is used to enforce the self-consistency on the impurity self-energy and the gap value. The approach gives the order parameter and the Green's function that can be used to determine the physical properties below.

### III. FERMI SURFACE, UPPER CRITICAL FIELD, AND MAKI PARAMETER

We consider a model Fermi surface that approximates the main sheet of $CeCoIn_5$ as seen by the magnetic oscillations.[39–41,61] It has the shape of an open cylinder rotationally symmetric in the $a$-$b$ plane (component of the momentum labeled $p_r$) and modulated along the $c$ axis[9] and is given by $p_f^2 = p_r^2 - r^2 p_f^2 \cos(2ap_c/r^2 p_f)$ with $r=a=0.5$. This choice of parameters gives a moderate anisotropy between transport coefficients in the $c$ direction and $a$-$b$ plane, close to that of $CeCoIn_5$ in the normal state.[62] With this definition, the typical quasiparticle velocity in the basal plane is $v_f = p_f/m$ and that along the $c$ axis, $v_{f,c} \sim a v_f = 0.5 v_f$.

We choose the $d_{x^2-y^2}$ symmetry of the order parameter and take a model separable pairing interaction $V(\mathbf{k},\mathbf{p}) = V_0 \mathcal{Y}(\hat{\mathbf{k}})\mathcal{Y}(\hat{\mathbf{p}}) \equiv V_0 \mathcal{Y}(\phi)\mathcal{Y}(\phi')$, where $\phi$ labels the azimuthal angle around the Fermi surface, and $\mathcal{Y}(\phi) = \sqrt{2}\cos 2\phi$. With this choice $\Delta(\mathbf{R},\hat{\mathbf{p}}) = \sqrt{2}\Delta(\mathbf{R})\cos 2\phi$. The dimensionless coupling constant $N_0 V_0$ determines the transition temperature of the pure sample, $T_{c0}$, which is suppressed by impurities to $T_c$; we use this latter $T_c$ as a unit of energy. Similarly, the natural unit for the magnetic field is the characteristic orbital scale, $B_0 = \Phi_0/2\pi\xi_0^2$, where $\Phi_0 = hc/2e$ is the flux quantum and $\xi_0 = \hbar v_f/2\pi T_c$ is the coherence length.

We measure the strength of the Zeeman term via a dimensionless parameter $Z = \mu B_0/2\pi T_c$ (Ref. 63) so that the Zeeman splitting of the energy levels in dimensionless units is $\mu B/(2\pi T_c) = ZB/B_0$. Since we expect the orbital critical field $H_{c2}^{orb}$ to be of order $B_0$, and the Pauli limit corresponds to $\mu H_P \sim \Delta_0 \sim T_c$, we find $H_{c2}^{orb}/H_P \sim Z$.

We first compute the upper critical field by solving the linearized, with respect to the order parameter, quasiclassical equations. Under the combined effect of the orbital and Zeeman field the transition for strong enough Pauli term becomes first order at low temperatures, $T < T^*$. We determine $T^*$ in the clean limit by evaluating where the $\Delta^4$-term coefficient in the free energy expansion becomes negative. The general free energy expansion can be obtained from Eq. (12), but it is complicated in a dirty $d$-wave superconductor,[64] and since the precise location of $T^*$ is not important for this work we will not look for it here. At lower temperatures, the transition line can only be determined from the full free energy functional, which needs to also account for the possible existence of the additional modulations in the Fulde-Ferrell-Larkin-Ovchinnikov (FFLO) phase.[42–44] While there are many indications that in $CeCoIn_5$ a new phase exists in the high-field, low-temperature range[35,65–69] the experiments on the vortex state anisotropy are generally carried out away from that range. Consequently, we do not consider the FFLO-type modulation here.

Figure 1 shows the upper critical field, $H_{c2}(T)$ for a pure system for two different field orientations ($c$ axis and the in plane along the gap maximum) and for different strength of the Zeeman splitting. Our results for $Z=0$ resemble the classical results by Helfand and Werthamer[70,71] (HW) with differences in profiles attributed to anisotropic gap and nonspherical FS. The important observation is that the shape of the temperature dependence of the upper critical field changes with increasing $Z$, and that the linear region of $H_{c2}(T) \sim 1 - T/T_c$ near $T_c$ rapidly shrinks, eventually leading to $H_{c2} \sim \sqrt{1 - T/T_c}$ dependence characteristic of the Pauli-limited field. Hence, as is shown in Fig. 1 a frequently used experimental estimate of the $H_{c2}^{orb}(T=0)$ based on the slope of the measured upper critical field near $T_c$ is not reliable for paramagnetically limited superconductors: that estimate changes on approaching the Pauli limit. First, the slopes $dH_{c2}/dT$ of the purely orbital and paramagnetically limited cases, while equal asymptotically as $T \to T_c$, are different when determined within a reasonable experimental window as shown by dotted lines based on the values of $H_{c2}$ at $T/T_c = (0.9, 1)$. We find that even for moderate paramagnetic coupling a reasonable estimate of the slope may be obtained only within a window of 1–3 % near $T_c$. Second, the $H_{c2}(T)$ profile for our chosen Fermi surface and the $d$-wave order parameter even for the purely orbital case is different from that found using the HW (Ref. 70) result for $s$-wave superconductor with a spherical FS with the same $dH_{c2}/dT(T_c)$. Consequently, for $Z \sim 1$ the estimate of $H_{c2}^{orb}$ using the HW profile and an approximate slope $dH_{c2}/dT(T_c)$ based on points more than a few percent away from $T_c$ may significantly underestimate the magnitude of $H_{c2}^{orb}$, as indicated by the arrows in Fig. 1.

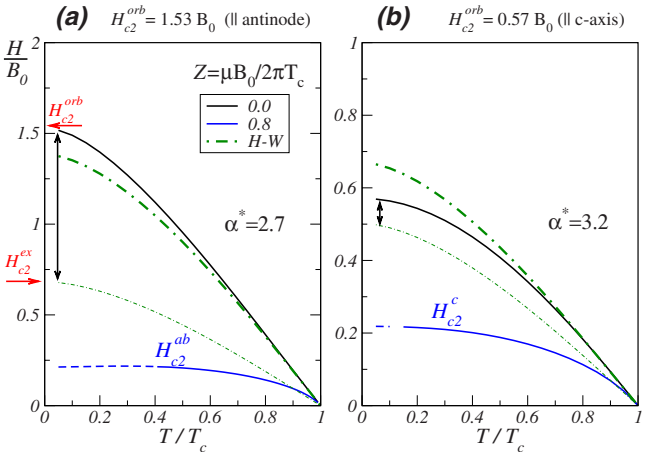


FIG. 1. (Color online) Difference between estimated and computed orbital upper critical field, $H_{c2}^{orb}$, in strongly paramagnetic superconductors for (a) in-plane field and (b) field normal to the planes. Lower solid lines denote $H_{c2}$ for the paramagnetically limiting case $Z=0.8$ and are continued as broken lines in regions of the first order transition. The orbital field is computed by ignoring Zeeman splitting ($Z=0$), the upper solid lines. It is in reasonable agreement with the values based on the HW result (Ref. 70), thick dot-dashed lines. If, however, the HW plot is based on the slope $dH_{c2}/dT$ at $T_c$ determined from the points $T/T_c = (0.9, 1)$ for $Z=0.8$, thin dot-dashed lines, the extracted orbital limit, $H_{c2}^{ex}$, is significantly different from $H_{c2}^{orb}$ as indicated by vertical arrows.

The change in the shape of the $H_{c2}(T)$ curve with increasing paramagnetic contribution is made even more explicit in

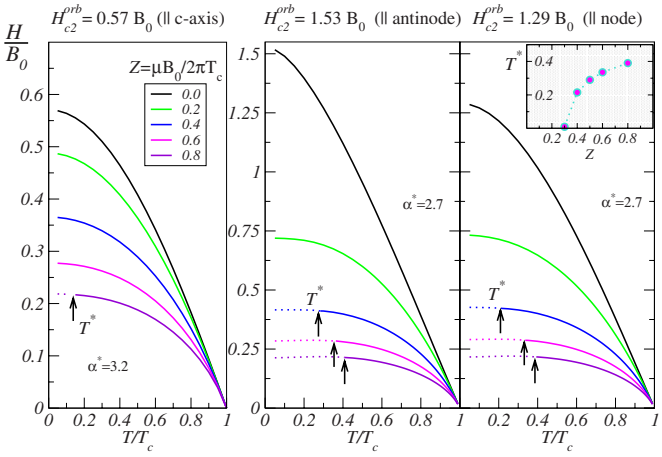


FIG. 2. (Color online) Upper critical field of a pure $d_{x^2-y^2}$ superconductor with quasicylindrical FS for three orientations of the field. The critical value of the Maki parameter is about $\alpha^* \sim 3$ for all directions (see text). The dotted lines indicate first order transition below $T^*$. Inset of the right-hand panel: $T^*$ as a function of the relative strength of the Pauli limiting. For purely Pauli-limited case $T_P^* \approx 0.56 T_c$.

Fig. 2, where we also include the upper critical field for the in-plane field along the nodal direction. As can be expected in a magnetically isotropic system, increased Pauli limiting reduces the anisotropy of the upper critical field caused by both the in-plane anisotropy of the order parameter (node vs antinode) and the anisotropy of the Fermi surface ($c$ axis vs $a$-$b$ plane).

Finally, in the inset of Fig. 2 we show the onset temperature for the first order transition, $T^*$ as a function of the Pauli limiting parameter $Z$. It is instructive to recast this analysis in terms of the so-called Maki parameter, $\alpha = \sqrt{2} H_{c2}^{orb} / H_P$. It is conventionally assumed that the critical value of the Maki parameter that defines a strong paramagnetic limit is $\alpha > \alpha^* = 1$, as obtained for the onset of the first order transition in $s$-wave superconductors with a spherical Fermi surface;[37] this value is commonly used in the analysis of anisotropic strongly correlated materials as well. In reality the critical value $\alpha^*$ depends on details of the Fermi surface and the superconducting state. For our model $H_{c2}^{orb} \sim 1.4$ in the $a$-$b$ plane and $\mu H_P \approx 1.11 \Delta_{d0} / \sqrt{2}$. Here $\Delta_{d0} = 0.241(2\pi T_c)$ is the amplitude of the order parameter at $T = H = 0$ (Ref. 72) and the increase in $H_P$ by factor 1.11 compared with the similar $s$-wave expression is caused by the gain in magnetic energy of the $d$-wave superconducting state by magnetization of the nodal quasiparticles.[73] The critical value of the Maki parameter where first order transition appears is therefore $\alpha^* = \sqrt{2} H_{c2}^{orb} / H_P \approx 7.0 (H_{c2}^{orb} / B_0) Z^*$ and since in-plane $Z^* \sim 0.3$ we have $\alpha_{d\text{-}wave}^* \approx 3.0$, significantly exceeding the value of unity expected for *dirty* isotropic systems.

We apply our results to $CeCoIn_5$ to analyze the behavior of the upper critical field along $a$ and $c$ axes. The fit for the [100] direction is shown in Fig. 3. The best fit of the second order transition and the location of $T^*$ in the experimental range is given by $Z^a \sim 0.5$. For $H \| c$ the best fit is given by $Z^c \sim 1.15$. From these two fits we obtain the value for $B_0$

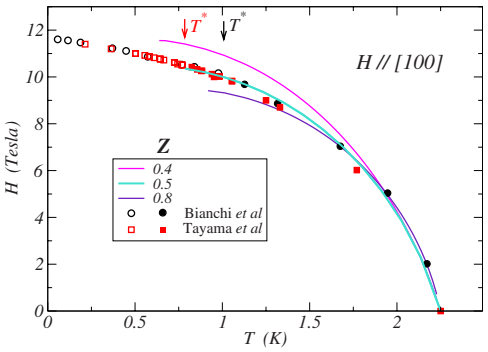


FIG. 3. (Color online) A fit of the experimental $H_{c2} \| [100]$ in $CeCoIn_5$. The data are taken from measurements of magnetization by Tayama *et al.* (Ref. 26) and specific heat by Bianchi *et al.* (Ref. 65). We find that $Z = 0.5$ gives the best fit of second order transition line and the onset of the first order transition $T^*$.

which is approximately 30 T for both field orientations, which is an indication that our choice of the FS parameters was reasonably good to describe this system. From this value we find the Fermi velocity $v_f \sim 0.6 \times 10^6$ cm/$s$, which is sensible for a heavy fermion system and agrees with interpretation of the experimental data[74] and disagrees with the value $\sim 10^8$ cm/$s$ obtained by authors of Ref. 44. We then extract the values of the effective electron moment, $\mu / \mu_B = Z(2\pi k_B T_c) / (\mu_B B_0)$ and obtain $\mu_{ab} / \mu_B \approx 0.35$ and $\mu_c / \mu_B \approx 0.7$, in agreement with Ref. 44 where the varying parameters were Fermi velocity and the $\mathfrak{g}$ factor.

We do note that in the current model the orbital pairbreaking is stronger for the nodal direction, Fig. 4(a), hence the Pauli effect is relatively less important and the range of first order transition is smaller for that orientation [Fig. 4(c)]. However, this particular aspect depends sensitively on the in-plane shape of the Fermi surface. We took the Fermi surface to be rotationally symmetric and the question of how

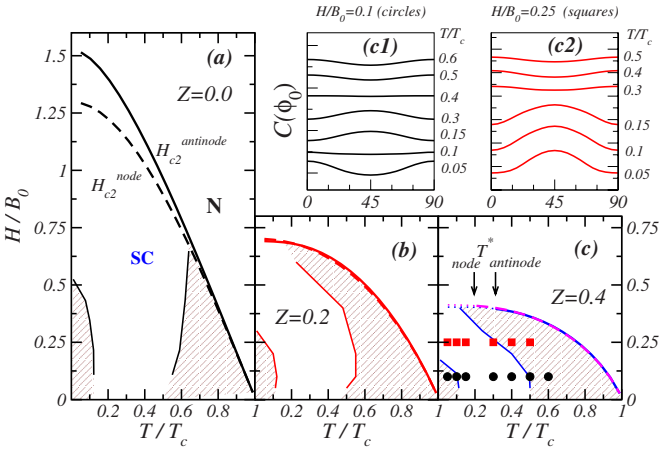


FIG. 4. (Color online) The anisotropy of heat capacity phase diagram for three Zeeman couplings (a) $Z = 0.0$, (b) $Z = 0.2$, and (c) $Z = 0.4$. Shaded areas correspond to minimum of the heat capacity for $\mathbf{H} \| (\text{node})$. Panels (c1) and (c2) demonstrate how anisotropy of heat capacity, $C(\phi_0)$, varies with temperature and magnetic field for $Z = 0.4$. The curves for different $T/T_c$ are shifted vertically for clarity.

this conclusion is affected by a more realistic Fermi surface shape is left for future studies.

## IV. TRANSPORT AND SPECIFIC HEAT ANISOTROPY

We are now in the position to analyze how the Pauli limiting affects the measured anisotropies of the specific heat, $C(\phi_0)$, and longitudinal thermal conductivity, $\kappa_{xx}(\phi_0)$, when magnetic field is rotated in the basal plane with respect to the crystalline axes. The direction of the field, $\phi_0$, is measured from the gap's maximum along the $a$ axis. As is well known, both quantities show oscillations, with either minima or maxima when the field is aligned with the nodal directions.[2,9–11,22,23] The location of the inversion line in the $T$-$H$ plane that separates the regions with minima and maxima indicating the gap nodes is of exceptional experimental relevance as it affects the conclusions about the shape of the gap in a given compound.

The results are most clearly presented in the form of a phase diagram in the $T$-$H$ variables that indicates each of the regions. In Fig. 4 we show the evolution of such phase diagram for the specific heat anisotropy with increasing Zeeman coupling. We compute the density of states, $N(\varepsilon,T)=-(N_0/2\pi)\langle \Im m g(\hat{\mathbf{p}},\varepsilon)\rangle_{\hat{\mathbf{p}}}$, where inclusion of $T$ signifies that the self-consistently determined gap is temperature dependent, obtain the entropy,

$$S(T,\mathbf{H}) = -\int_{-\infty}^{\infty} d\varepsilon N(\varepsilon,T)\{f(\varepsilon)\ln f(\varepsilon) + [1-f(\varepsilon)]\ln[1-f(\varepsilon)]\} \tag{14}$$

and numerically differentiate it to find $C/T$. The result for purely orbital coupling to magnetic field, $Z=0.0$ in Fig. 4(a) is in agreement with Ref. 10: In the two shaded regions (near $H_{c2}$ and in low-$T$ low-$H$ corner) the heat capacity attains its minimum when the field is along the nodal directions of the gap. Clearly, since the anisotropy in the heat capacity is field induced, the amplitude of the anisotropy is very small at low fields for all temperatures and extremely small near $T_c$. Hence the challenge is to go to sufficiently high fields to see the signal while knowing whether the maximum or a minimum of the anisotropic signal corresponds to the nodal directions.

As the relative strength of the spin coupling increases, Figs. 4(b) and 4(c), we note that the "nodal minimum" region near $H_{c2}$ grows at the expense of the intermediate field unshaded region. This is concomitant with the disappearance of the anisotropy of the upper critical fields for nodal and antinodal directions. An obvious conjecture is that for $Z=0$ at intermediate temperatures and *moderately high fields* it is the anisotropy of the upper critical field that controls the anisotropy of the specific heat: since $H_{c2}^{node}<H_{c2}^{antinode}$, at a fixed external field $H/H_{c2}^{node}>H/H_{c2}^{antinode}$, and the density of states, along with the heat capacity, is higher for the field along the nodal direction. As the Zeeman coupling is increased and the critical fields along the nodal and the antinodal directions become nearly equal, this unshaded region shrinks. In Fig. 4(c) we tuned $Z>Z^*$ and see that the critical fields for the two in-plane directions are almost indistinguishable, and that there is a region of first order transition at low temperatures $T<T^*$, indicated by the arrows.

Importantly for our purposes, the low-$T$, low-$H$ shaded region (minima for the field along the nodes) remains mostly unchanged with increasing $Z$, terminating at $T/T_c\sim 0.1$ and $H/H_{c2}^{Z}\sim 0.4$. This region is still dominated by the nodal quasiparticles and "semiclassical" physics, $N(0,H)\sim\sqrt{H/H_{c2}^{orb}}$,[75,76] compared to a linear contributions due to Zeeman shifts (for these $Z$'s) and vortex cores.

Figures 4(c1) and 4(c2) provide the profiles of the heat capacity anisotropy for $Z=0.4$ and two different fields at locations indicated by circles and squares correspondingly. The heat capacity expression that we use to plot the angular dependence,

$$C(T,\mathbf{H}) = \int_{-\infty}^{\infty} \frac{\varepsilon^2 d\varepsilon}{4T^2} \frac{N_\uparrow(\varepsilon,T,\mathbf{H}) + N_\downarrow(\varepsilon,T,\mathbf{H})}{\cosh^2(\varepsilon/2T)}, \tag{15}$$

is, strictly speaking, valid only at low temperature when the order parameter is essentially temperature independent. The difference between this expression and the exact result obtained from the entropy differentiation is small far from the superconducting transition, see Refs. 9 and 10.

We also compute the anisotropy of the thermal conductivity along the crystalline $x$ direction for unitarity scattering (phase shift $\pi/2$) and the normal state scattering rate $\Gamma/2\pi T_c=0.007$. The thermal conductivity is calculated on equal footing with the density of states[11,52] and is given by $\kappa_{ij}=\kappa_{ij,\uparrow}+\kappa_{ij,\downarrow}$, where the spin direction $s=\uparrow,\downarrow$ and

$$\frac{\kappa_{xx,s}(T,H)}{T} = \int_{-\infty}^{+\infty} \frac{d\varepsilon}{2T}\frac{\varepsilon^2}{T^2}\cosh^{-2}\frac{\varepsilon}{2T} \times \langle v_{f,x}^2 N_s(T,\mathbf{H};\hat{\mathbf{p}},\varepsilon)\tau_{H,s}(T,H;\hat{\mathbf{p}},\varepsilon)\rangle_{\hat{\mathbf{p}}} \tag{16}$$

with the effective scattering rate

$$\frac{1}{2\tau_{H,s}} = -\Im m\Sigma_s^R + \sqrt{\pi}\frac{2\Lambda}{|\tilde{v}_f^\perp|}\frac{\Im m[g_s^R W(2\tilde{\varepsilon}\Lambda/|\tilde{v}_f^\perp|)]}{\Im m g_s^R}|\Delta_0\mathcal{Y}|^2. \tag{17}$$

Here the label $R$ denotes a retarded function and we use the angle-resolved density of states.

Figure 5 shows characteristic profiles of the heat capacity and heat conductivity when the field is rotated in the basal plane. Note that in the left panel we labeled the fields according to the ratio $H/H_{c2}$: the upper critical field changes between $Z=0$ and 0.4 so that the effective field range is different. As discussed above, the major difference between two values of the Zeeman splitting is that for higher $Z$ there exists a region of shallow minimum at the node (45° in our case) for high fields.

The second panel of Fig. 5 shows the behavior of the thermal conductivity for the same fields, now labeled in units of $B_0$. Qualitatively, the peak in the angle dependent $\kappa$ for $Z=0$ at 45° disappears at $Z=0.4$, making the dependence of the thermal conductivity more twofold.

To quantify these trends we follow the approaches taken in experiment and expand both quantities in harmonics of the angle between the field and the heat current,

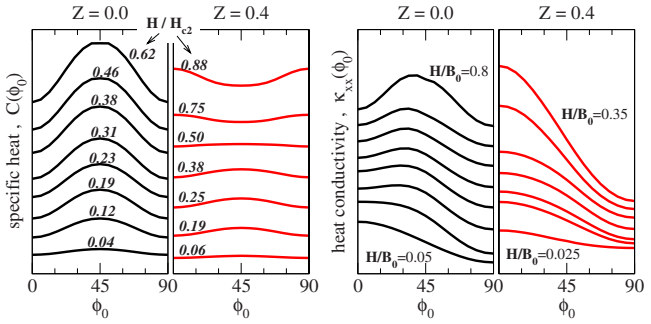


FIG. 5. (Color online) Anisotropy of the specific heat (left) and heat conductivity (right) for $Z=0.0$ and 0.4 at $T/T_c=0.3$ and various fields. The field values are shown on the left in terms of $Z$-dependent $H_{c2}$. The curves were shifted vertically for clarity. The absolute values of $C$ and $\kappa$ and their anisotropies are presented in Figs. 6–9 below. The range of fields in $H/B_0$ for convenience indicated on the right.

$$\frac{C(\phi_0,T,H)/T}{(C/T)_N} = C_{0\phi} + C_{4\phi}\cos 4\phi_0,$$

$$\frac{\kappa_{xx}(\phi_0,T,H)/T}{(\kappa_{xx}/T)_N} = \kappa_{0\phi} + \kappa_{2\phi}\cos 2\phi_0 + \kappa_{4\phi}\cos 4\phi_0 \tag{18}$$

and present the evolution of different coefficients with field and temperature.

First, focus on the behavior of the specific heat as shown in Fig. 6. At low fields for $Z=0$ the isotropic part, $C_{0\phi}$, shown in panels (a) and (c), exhibits the approximate $\sqrt{H}$ behavior expected of a nodal superconductor.[75,77] With increased Zeeman contribution this component of the specific

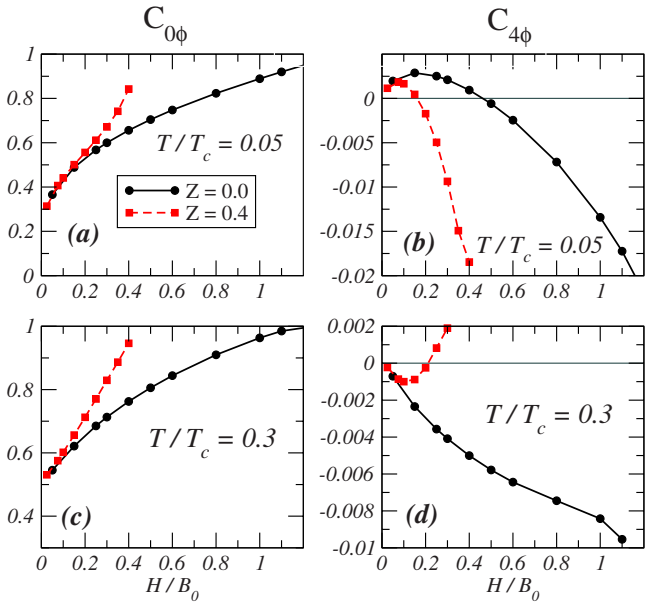


FIG. 6. (Color online) $C_{0\phi}$ and $C_{4\phi}$ coefficients in heat capacity expansion at two different temperatures, $T=0.05T_c$ and $T=0.3T_c$. Positive fourfold coefficient means that the specific heat has minimum for the field along a node in the gap while negative $C_{4\phi}$ corresponds to the maximum for the field along a node.

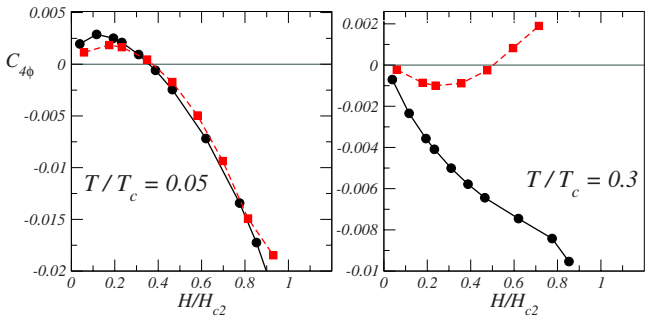


FIG. 7. (Color online) The anisotropic component of the specific heat at temperatures $T=0.05T_c$ (left panel) and $T=0.3T_c$ (right panel) for $Z=0$ and 0.4.

heat becomes more linear in field.[3,78] This is, of course, simply because the spin-split quasiparticle spectra produce a density of states at zero energy, $N(0,H)\simeq(\mu H)/\Delta_0$, with the prefactor that, for high $\mu$, can be large enough to dominate the sublinear Volovik term already at low fields. At low temperatures $C_{0\phi}$ acquires a positive curvature at high fields, in agreement with Ref. 63.

The qualitative behavior of the anisotropic term, $C_{4\phi}$, is similar for the two values of $Z$ at low temperature, panel (b), but is distinctly smaller at higher temperature, shown in panel (d), and even changes sign near $H_{c2}$. The comparison becomes even more clear if the amplitude $C_{4\phi}$ is plotted against the upper critical field for given values of Zeeman splitting, as in Fig. 7. At low temperature there is essentially no difference between the purely orbital case and that of a moderately strong Zeeman coupling and hence in this regime the anisotropy depends only on the shape of the gap and the underlying Fermi surface. In contrast, at $T/T_c=0.3$ for the case of weak Zeeman splitting the coefficient does not change sign, as seen already from Fig. 4(a). In contrast, for $Z=0.4$ as shown in Fig. 4(c), there is a change of sign in the anisotropy of the specific heat due to the "isotropization" of the upper critical field, as discussed above.

The same trend is seen in the thermal transport anisotropy. The behavior of the average thermal conductivity, $\kappa_0$ and the twofold term responsible for the difference between heat transport parallel and perpendicular to the vortices, is shown in Fig. 8. At low fields the scattering of the quasiparticles on the vortices is determined by the vortex concentration, $n \sim H/\Phi_0$, and therefore, at low temperature, only weakly depends on the Zeeman field. As the temperature increases, however, the differences between the two cases become much more pronounced. In particular, it is worth noting that the twofold symmetry $\kappa_{2\phi}>0$ $[\kappa_{xx}(\mathbf{j}_h\|\mathbf{H})>\kappa_{xx}(\mathbf{j}_h\perp\mathbf{H})]$ is much more pronounced in the Pauli-limited case.

The fourfold "nodal" term, Fig. 9, shows the behavior broadly similar to that of the anisotropic component of the specific heat. The low-temperature behavior as a function of the reduced field, $H/H_{c2}$ is similar for the cases of weak and strong Pauli limiting while the behavior at moderate temperatures is very different starting at moderate fields. Once again, the coefficients for $Z=0$ and 0.4 have the opposite signs starting at $H\sim 0.5H_{c2}$.

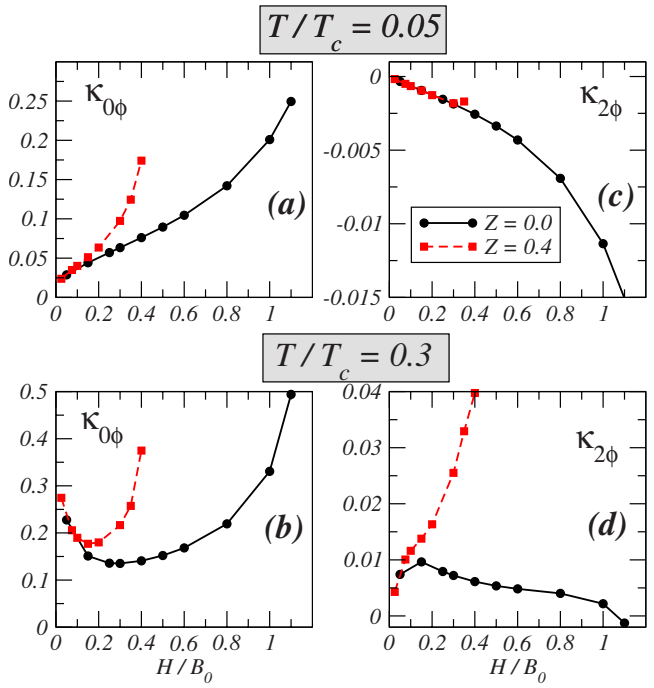


FIG. 8. (Color online) Field dependence of the coefficients $\kappa_0$ and $\kappa_2$ in the expansion of the thermal conductivity, Eq. (18) at $T=0.05T_c$ (top two panels), and $T=0.3T_c$ (bottom panels) for $Z=0$ and 0.4.

## V. CONCLUSIONS

In conclusion, we calculated in a $d$-wave superconductor with quasicylindrical FS the $H_{c2}$ and its evolution for transition between orbital and Pauli limits. We find that in this system the critical value of the Maki parameter for paramagnetic limit criterion is $\alpha^*=3$. That values depends on both the symmetry of the order parameter and the shape of the Fermi surface, and hence there is no universal threshold value for that parameter that ensures the first order transition in a given system. We also find that the linear extrapolation of the upper critical field in Pauli-limited superconductors from the vicinity of $T_c$ to low temperatures does not accurately predict the value of the orbital critical field.

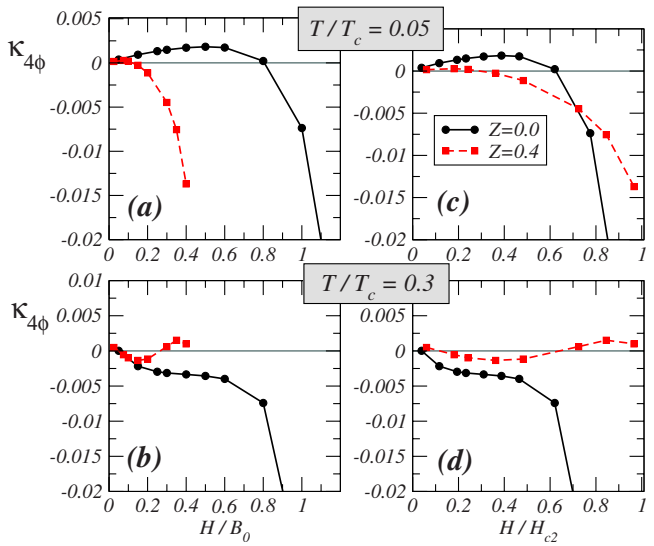


FIG. 9. (Color online) The anisotropic fourfold term of the thermal conductivity in Eq. (19) is shown for $T=0.05T_c$ in panels (a) and (c), and for $T=0.3T_c$ in panels (b) and (d) as function of the field, panels (a) and (b) and the reduced field, $H/H_{c2}$, panels (c) and (d).

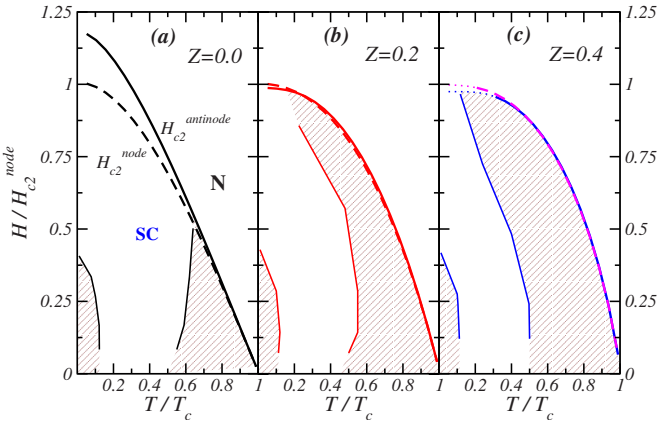


FIG. 10. (Color online) The phase diagram for the anisotropy of the specific heat under rotated magnetic field for different strength of Pauli pairbreaking term. Shaded areas correspond to minimum of the heat capacity for $\mathbf{H}\|$(node). Notice that the shaded region at low $T$ and $H$ is identical in all three panels.

We showed that moderately large Zeeman contribution does not alter the typical behavior of $C$ and $\kappa$ anisotropy at low temperatures and fields. This is summarized in the phase diagram in Fig. 10. The region at low $T$ and $H$ where the minima in the fourfold terms in the heat capacity and thermal conductivity occur for the field along the nodes is essentially insensitive to the strength of the Zeeman coupling. The differences, of course, occur at higher temperatures and fields.

This finding proves that, even in systems with strong paramagnetic contribution where $H_{c2}$ anisotropy in the $a$-$b$ plane is largely absent and therefore cannot be used to infer the nodal structure,[79] the anisotropy of heat conductivity and heat capacity at moderate to low $H$ and $T$ still can help determine the location of the nodes of the order parameter on the Fermi surface. The previous analysis[9] of the inversion of the anisotropy in $CeCoIn_5$ remains valid when the Zeeman term is accounted for and unequivocally indicates the $d_{x^2-y^2}$ shape of the order parameter. This also provides further support for the interpretation of Ref. 25 that confirmed the inversion of the specific heat oscillations. Of course, further studies incorporating the shape of the Fermi surface specific to the 115-family are needed for detailed comparison of the location of the experimentally determined inversion line with theoretical predictions.

## ACKNOWLEDGMENTS

This research was supported in part by the U.S. Department of Energy under Grant No. DE-FG02-08ER46492. We are also grateful for the hospitality of the Aspen Center for Physics, where part of this work was done.

[1] M. Tinkham, *Introduction to Superconductivity* (Robert E. Krieger, Malabar, Florida, 1985).
[2] I. Vekhter, P. J. Hirschfeld, J. P. Carbotte, and E. J. Nicol, Phys. Rev. B **59**, R9023 (1999).
[3] I. Vekhter, P. J. Hirschfeld, and E. J. Nicol, Phys. Rev. B **64**, 064513 (2001).
[4] H. Won and K. Maki, Europhys. Lett. **56**, 729 (2001).
[5] P. Thalmeier and K. Maki, Europhys. Lett. **58**, 119 (2002).
[6] P. Miranović, N. Nakai, M. Ichioka, and K. Machida, Phys. Rev. B **68**, 052501 (2003).
[7] N. Nakai, P. Miranovic, M. Ichioka, and K. Machida, Phys. Rev. B **70**, 100503(R) (2004).
[8] P. Miranović, M. Ichioka, K. Machida, and N. Nakai, J. Phys.: Condens. Matter **17**, 7971 (2005).
[9] A. B. Vorontsov and I. Vekhter, Phys. Rev. Lett. **96**, 237001 (2006).
[10] A. B. Vorontsov and I. Vekhter, Phys. Rev. B **75**, 224501 (2007).
[11] A. B. Vorontsov and I. Vekhter, Phys. Rev. B **75**, 224502 (2007).
[12] G. R. Boyd, P. J. Hirschfeld, I. Vekhter, and A. B. Vorontsov, Phys. Rev. B **79**, 064525 (2009).
[13] T. Park, M. B. Salamon, E. M. Choi, H. J. Kim, and S.-I. Lee, Phys. Rev. Lett. **90**, 177001 (2003).
[14] T. Park and M. B. Salamon, Mod. Phys. Lett. B **18**, 1205 (2004).
[15] H. Aoki, T. Sakakibara, H. Shishido, R. Settai, Y. Onuki, P. Miranović, and K. Machida, J. Phys.: Condens. Matter **16**, L13 (2004).
[16] F. Yu, M. B. Salamon, A. J. Leggett, W. C. Lee, and D. M. Ginsberg, Phys. Rev. Lett. **74**, 5136 (1995); **75**, 3028(E) (1995).
[17] H. Aubin, K. Behnia, M. Ribault, R. Gagnon, and L. Taillefer, Phys. Rev. Lett. **78**, 2624 (1997).
[18] T. Watanabe, K. Izawa, Y. Kasahara, Y. Haga, Y. Onuki, P. Thalmeier, K. Maki, and Y. Matsuda, Phys. Rev. B **70**, 184502 (2004).
[19] K. Izawa, K. Kamata, Y. Nakajima, Y. Matsuda, T. Watanabe, M. Nohara, H. Takagi, P. Thalmeier, and K. Maki, Phys. Rev. Lett. **89**, 137006 (2002).
[20] K. Izawa, H. Yamaguchi, T. Sasaki, and Y. Matsuda, Phys. Rev. Lett. **88**, 027002 (2001).
[21] K. Izawa, H. Yamaguchi, Y. Matsuda, H. Shishido, R. Settai, and Y. Onuki, Phys. Rev. Lett. **87**, 057002 (2001).
[22] Y. Matsuda, K. Izawa, and I. Vekhter, J. Phys.: Condens. Matter **18**, R705 (2006).
[23] T. Sakakibara, A. Yamada, J. Custers, K. Yano, T. Tayama, H. Aoki, and K. Machida, J. Phys. Soc. Jpn. **76**, 051004 (2007).
[24] K. Yano, T. Sakakibara, T. Tayama, M. Yokoyama, H. Amitsuka, Y. Homma, P. Miranović, M. Ichioka, Y. Tsutsumi, and K. Machida, Phys. Rev. Lett. **100**, 017004 (2008).
[25] K. An, T. Sakakibara, R. Settai, Y. Onuki, M. Hiragi, M. Ichioka, and K. Machida, Phys. Rev. Lett. **104**, 037002 (2010).
[26] T. Tayama, A. Harita, T. Sakakibara, Y. Haga, H. Shishido, R. Settai, and Y. Onuki, Phys. Rev. B **65**, 180504(R) (2002).
[27] A. Bianchi, R. Movshovich, N. Oeschler, P. Gegenwart, F. Steglich, J. D. Thompson, P. G. Pagliuso, and J. L. Sarrao, Phys. Rev. Lett. **89**, 137002 (2002).
[28] A. D. Bianchi *et al.*, Science **319**, 177 (2008).
[29] B. Chandrasekhar, Appl. Phys. Lett. **1**, 7 (1962).
[30] A. Clogston, Phys. Rev. Lett. **9**, 266 (1962).
[31] P. M. Tedrow, R. Meservey, and B. B. Schwartz, Phys. Rev. Lett. **24**, 1004 (1970).
[32] W. Wu, R. G. Goodrich, and P. W. Adams, Phys. Rev. B **51**, 1378 (1995).
[33] P. W. Adams, P. Herron, and E. I. Meletis, Phys. Rev. B **58**, R2952 (1998).
[34] M. Ichioka and K. Machida, Phys. Rev. B **76**, 064502 (2007).
[35] C. Capan, A. Bianchi, R. Movshovich, A. D. Christianson, A. Malinowski, M. F. Hundley, A. Lacerda, P. G. Pagliuso, and J. L. Sarrao, Phys. Rev. B **70**, 134513 (2004).
[36] L. W. Gruenberg and L. Gunther, Phys. Rev. Lett. **16**, 996 (1966).
[37] K. Maki, Phys. Rev. **148**, 362 (1966).
[38] D. Hall, E. C. Palm, T. P. Murphy, S. W. Tozer, Z. Fisk, U. Alver, R. G. Goodrich, J. L. Sarrao, P. G. Pagliuso, and T. Ebihara, Phys. Rev. B **64**, 212508 (2001).
[39] R. Settai, H. Shishido, S. Ikeda, Y. Murakawa, M. Nakashima, D. Aoki, Y. Haga, H. Harima, and Y. Onuki, J. Phys.: Condens. Matter **13**, L627 (2001).
[40] Y. Haga, Y. Inada, H. Harima, K. Oikawa, M. Murakawa, H. Nakawaki, Y. Tokiwa, D. Aoki, H. Shishido, S. Ikeda, N. Watanabe, and Y. Ōnuki, Phys. Rev. B **63**, 060503(R) (2001).
[41] N. Harrison *et al.*, Phys. Rev. Lett. **93**, 186405 (2004).
[42] H. Adachi and R. Ikeda, Phys. Rev. B **68**, 184510 (2003).
[43] R. Ikeda and H. Adachi, Phys. Rev. B **69**, 212506 (2004).
[44] H. Won, K. Maki, S. Haas, N. Oeschler, F. Weickert, and P. Gegenwart, Phys. Rev. B **69**, 180504(R) (2004).
[45] G. Eilenberger, Z. Phys. **214**, 195 (1968).
[46] A. I. Larkin and Y. N. Ovchinnikov, Sov. Phys. JETP **28**, 1200 (1969).
[47] J. A. X. Alexander, T. P. Orlando, D. Rainer, and P. M. Tedrow, Phys. Rev. B **31**, 5811 (1985).
[48] J. W. Serene and D. Rainer, Phys. Rep. **101**, 221 (1983).
[49] P. J. Hirschfeld, P. Wölfle, and D. Einzel, Phys. Rev. B **37**, 83 (1988).
[50] C. T. Rieck, K. Scharnberg, and N. Schopohl, J. Low Temp. Phys. **84**, 381 (1991).
[51] U. Klein, Phys. Rev. B **69**, 134518 (2004).
[52] I. Vekhter and A. Houghton, Phys. Rev. Lett. **83**, 4626 (1999).
[53] U. Brandt, W. Pesch, and L. Tewordt, Z. Phys. **201**, 209 (1967).
[54] W. Pesch, Z. Phys. B **21**, 263 (1975).
[55] I. A. Luk'yanchuk and V. P. Mineev, Zh. Eksp. Teor. Fiz. **93**, 2045 (1987) [Sov. Phys. JETP **66**, 1168 (1987)].
[56] H. Won and K. Maki, Phys. Rev. B **53**, 5927 (1996).
[57] E. H. Brandt, Rep. Prog. Phys. **58**, 1465 (1995).
[58] T. Dahm, S. Graser, C. Iniotakis, and N. Schopohl, Phys. Rev. B **66**, 144515 (2002).
[59] M. Udagawa, Y. Yanase, and M. Ogata, Phys. Rev. B **70**, 184515 (2004).
[60] G. Eilenberger, Phys. Rev. **153**, 584 (1967).
[61] H. Shishido *et al.*, J. Phys. Soc. Jpn. **71**, 162 (2002).
[62] A. Malinowski, M. F. Hundley, C. Capan, F. Ronning, R. Movshovich, N. O. Moreno, J. L. Sarrao, and J. D. Thompson, Phys. Rev. B **72**, 184506 (2005).
[63] H. Adachi, M. Ichioka, and K. Machida, J. Phys. Soc. Jpn. **74**, 2181 (2005).
[64] A. B. Vorontsov, I. Vekhter, and M. J. Graf, Phys. Rev. B **78**, 180505(R) (2008).
[65] A. Bianchi, R. Movshovich, C. Capan, P. G. Pagliuso, and J. L. Sarrao, Phys. Rev. Lett. **91**, 187004 (2003).
[66] T. Watanabe, Y. Kasahara, K. Izawa, T. Sakakibara, Y. Matsuda, C. J. van der Beek, T. Hanaguri, H. Shishido, R. Settai, and Y. Onuki, Phys. Rev. B **70**, 020506(R) (2004).

[67] C. Martin, C. C. Agosta, S. W. Tozer, H. A. Radovan, E. C. Palm, T. P. Murphy, and J. L. Sarrao, Phys. Rev. B **71**, 020503(R) (2005).
[68] V. F. Mitrović, M. Horvatić, C. Berthier, G. Knebel, G. Lapertot, and J. Flouquet, Phys. Rev. Lett. **97**, 117002 (2006).
[69] Y. Matsuda and H. Shimahara, J. Phys. Soc. Jpn. **76**, 051005 (2007).
[70] E. Helfand and N. R. Werthamer, Phys. Rev. **147**, 288 (1966).
[71] E. Helfand and N. R. Werthamer, Phys. Rev. Lett. **13**, 686 (1964).
[72] A. B. Vorontsov, J. A. Sauls, and M. J. Graf, Phys. Rev. B **72**, 184501 (2005).
[73] A. B. Vorontsov and M. J. Graf, Phys. Rev. B **74**, 172504 (2006).
[74] R. Movshovich, M. Jaime, J. D. Thompson, C. Petrovic, Z. Fisk, P. G. Pagliuso, and J. L. Sarrao, Phys. Rev. Lett. **86**, 5152 (2001).
[75] G. E. Volovik, JETP Lett. **58**, 469 (1993).
[76] V. Mineev and K. Samokhin, *Introduction to Unconventional Superconductivity* (Gordon and Breach, New York, 1999).
[77] C. Kübert and P. J. Hirschfeld, Solid State Commun. **105**, 459 (1998).
[78] K. Yang and S. L. Sondhi, Phys. Rev. B **57**, 8566 (1998).
[79] F. Weickert, P. Gegenwart, H. Won, D. Parker, and K. Maki, Phys. Rev. B **74**, 134511 (2006).